GEO-HEAT CENTER

Oregon Institute of Technology, Klamath Falls, Oregon 97601 541/885-1750 FAX 541/885-1754

John W. Lund, Director
Andrew Chiasson
Tonya "Toni" Boyd
Debi Carr

September 30, 2006

This work has been funded and completed under Midwest Research Institute, National Renewable Energy Laboratory (NREL) Task Order No. KLDJ-5-55052-02, "*Technical Assistance with Direct Use Projects in Oregon and Nevada*", Task 2: Geothermal Industrial Park – Elko, NV.

Project Background

The Elko Heat Company has been operating a geothermal district heating system in Elko, NV since December 1982. An artesian production well supplies water to customers at approximately 178°F with an artesian flow rate of 425 gpm. Currently, an industrial park is under construction to use return water from the Elko Heat Company's district heating system. Figure 1 is a Google Earth photo of the project site.

Figure 1. Aerial photo of the project site.

Development plans for the Geothermal Industrial Park first called for the construction of a pump house, which will boost the pressure of the return flow from the existing Elko Heat Company system from 10-15 psi up to 40-50 psi to circulate this water through the 20 acre industrial park. The return water from the Elko Heat Company district heating system is typically at 120 to 130^{o}F. The pump house will also have capacity to circulate water over a "water fall" serving a cooling pond and fountain and be capable of providing irrigation flow to the park landscaping.

The first planned building is 33,600 ft^2 concrete tilt-up construction with 24 ft clear warehouse space. The tenants were anticipated to require 15 to 20% of the occupied space as office and the balance as warehouse use. The office space is to be heated by radiant floor methods and the warehouse space with fan coils. It is also planned to cascade the space heat to a snow melt system at the entrances to the building.

At the time of completion of this report, either all the space had been leased or final negotiations were in progress. Names of lease holders were not available at this time due to confidentiality reasons. Tenants will be required to share in the maintenance, insurance, taxes, and utility and other building and site landscaping costs. As an incentive, free heat will be provided for the first few years, during which time a Btu metering system will be developed.

Objectives and Scope

The objectives of this Task Ordering Agreement were to provide technical assistance to the developers of the Geothermal Industrial Park of Elko. The technical assistance tasks included a site visit, review of construction plans, suggestions for possible tenants, suggested uses of the geothermal energy, possible avenues for obtaining renewable energy credits, and analysis of a supplemental heat rejection system.

Much of the technical assistance was handled via email or telephone conversations. This report summarizes the Geo-Heat Center's review of the construction drawings and an analysis of the supplemental heat rejection system.

Review of Construction Drawings

Canyon Engineering provided the Geo-Heat Center with the following Phase I construction drawings (May 19, 2006):

- Pond/Pump Station (Sheets 1-4)
- Elko Industrial Park (Sheets (1-4)
- Elko Geothermal Industrial Park Site Plans (two sheets)

The following comments and suggestions were made regarding the proposed radiant slab heating system. The drawings show a "single serpentine" arrangement for all radiant floor heating and snow melting. There are optimal ways of laying out the tubing in rooms, depending on the number of exterior walls. Snow melting tubing is laid out in yet a different arrangement. In radiant floor heating of rooms, it is more desirable to place the hottest water near the exterior walls. In snow melting, the goal is to get an even distribution of heat across the slab. Suggested tubing arrangements are shown in the following sketches.

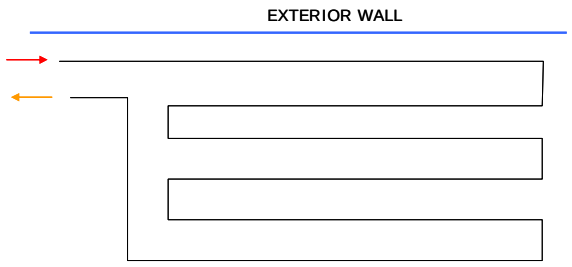

(a) one exterior wall

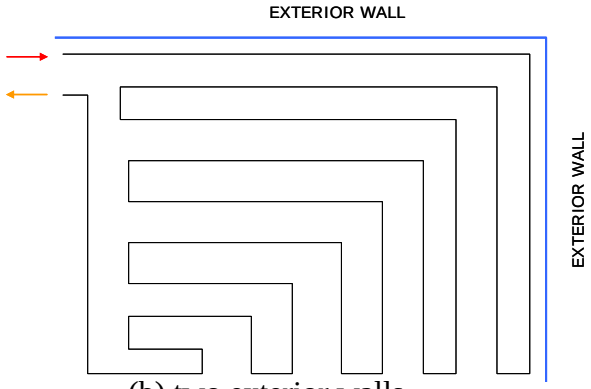

(b) two exterior walls

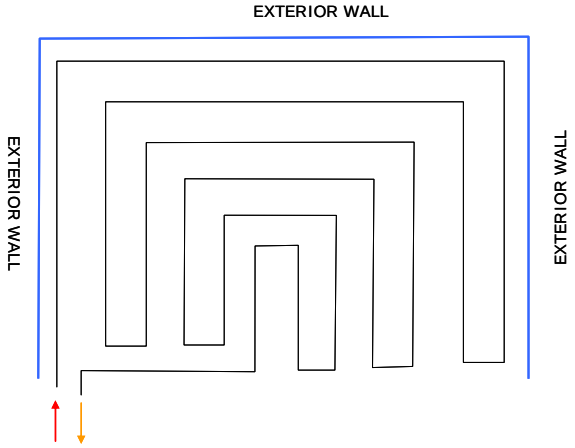

(d) three exterior walls

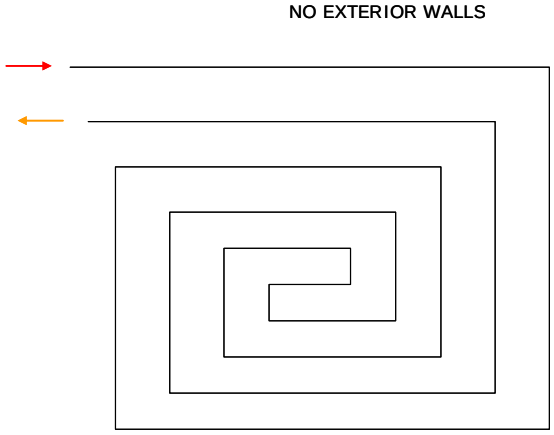

(e) no exterior walls

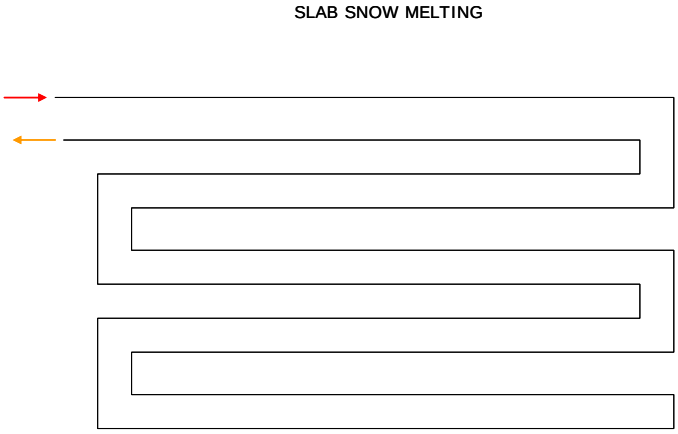

(f) snow melting

Figure 2. Radiant slab tubing layout.

The following suggestions were made regarding outdoor air handling. With radiant floor heating systems, outdoor ventilation air must be brought in by a separate system. ASHRAE Standard 62-1999 (updated since then) recommends 20 cfm outdoor air per person for office spaces, and the net occupiable space for an office is 7 persons per 1000 ft^2. So, in a 5,000 ft^2 office, you might need to bring in 700 cfm outdoor air.

The roof top units on the drawings specify electric heat. As an energy-savings measure, you might consider substituting these with roof-top heat recovery ventilators. These can be ordered with DX cooling coils and hot water heating coils. The DX cooling coils will provide all cooling, and the hot water heating coils (with the heat provided by the geothermal water) will just do outdoor air pre-heating on the coldest days. Example manufacturers of these types of units are Venmar or Semco. These systems typically have a payback of less than 5 years.

Analysis of Supplemental Heat Rejection System

This section describes our analysis of a "supplemental heat rejection system" planned for the new Geothermal Industrial Park in Elko, NV. The purpose of the supplemental heat rejection system is to reduce geothermal water temperature prior to discharging the water. The objective of our analysis is to estimate how much the geothermal temperature can actually be decreased, and to recommend improvements on the design for future construction.

Heat Rejection System Description: The supplemental heat rejection system is a buried horizontal network of 2-inch nominal diameter HDPE pipe. The pipe is to be buried below an asphalt parking lot with a plan area of 60 ft x 100 ft. The pipe burial depth is 12 in. below the surface, with a pipe-to-pipe spacing of 4 ft. The asphalt will be 2½ in. thick, and the pipe will be laid in crushed aggregate type fill. Approximately 40 gpm of geothermal fluid at 100^oF is expected to be available to flow through the piping network.

Approach: To analyze the heat rejection system properly, we used a detailed computer model developed for TRNSYS (acronym for transient systems simulation software). Model documentation is described in a paper published in the Journal of Solar Energy Engineering, which is attached as Appendix A.

In summary, the computer model performs an hourly energy balance on a horizontal earth cross-section with embedded piping. The top surface heat fluxes are due to environmental heat transfer processes, and are driven by hourly typical meteorological data. In this case, we obtained TMY (typical meteorological year) data for Elko, which is the same data file used for building loads and energy calculations. Conduction heat transfer through the subsurface materials is calculated with a finite difference method. Hourly fluid temperatures are then determined by an energy balance on the fluid. Input data to the model, in addition to weather data, includes cross-section geometry and thermal properties.

Results: The results are presented on a series of graphs below (labeled Figures 3-5), showing hourly fluid temperatures exiting the supplemental heat rejection system. A sensitivity analysis was done on the fluid flow rate, pipe burial depth, and pipe spacing. The heat rejection system described above will be referred to as the **base case**. The results are summarized as follows:

- The base design (shown in blue on all graphs) will reduce the geothermal fluid temperature to about 92°F to 95°F in the winter and late fall months. During spring and early fall months, the geothermal fluid outlet temperature is above 95°F, and sometimes creeps above 100°F, due to the hot pavement surface temperature, especially in mid summer. However, the model made no allowance for shading from parked cars, but even so, during summer months, it is likely that it will only be possible to reject heat during cool nights.
- As may be expected, the parameter having the greatest influence on the exiting fluid temperature is the flow rate. As seen in Figure 3, decreasing the flow rate to 30 gpm lowers the exiting geothermal fluid temperature a few degrees in winter, but increases it slightly in summer. Obviously, decreasing the fluid flow rate means less water would be processed through the supplemental heat rejection system.
- A sensitivity on the pipe burial depth shows that 12 in. is a good choice. A pipe burial depth of 6 in. has some benefit of lowering the exiting geothermal fluid temperature during cold times, but these benefits are offset by higher geothermal exiting temperatures more hours during the year.
- A sensitivity on the pipe spacing shows that 4 ft is a good choice. There are some minor improvements in a 6 ft spacing, but 2 ft spacing shows considerable thermal interference and would not be recommended.

Figure 3. Sensitivity to Flow Rate

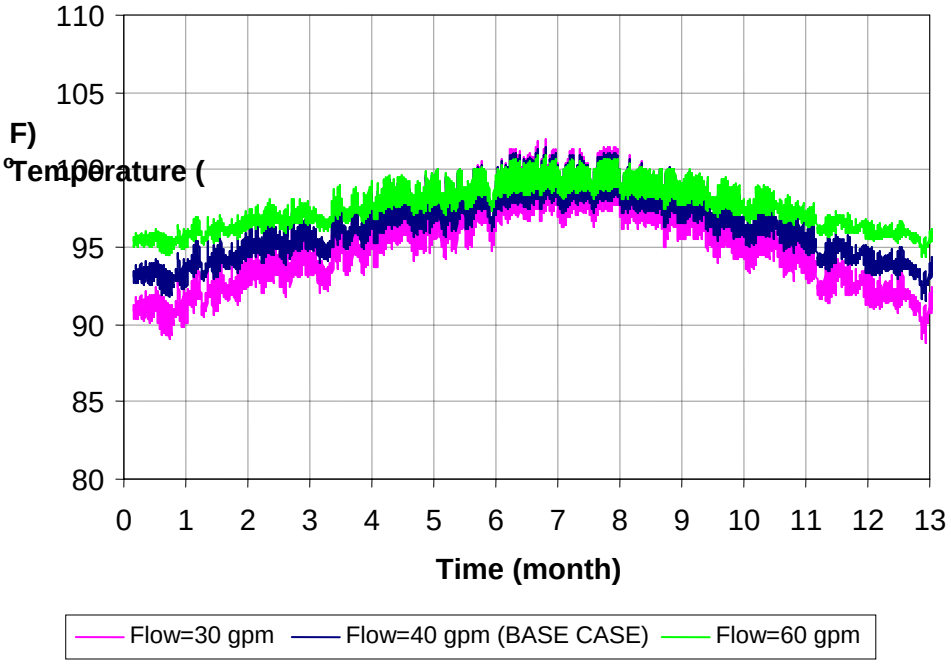

Figure 4. Sensitivity to Pipe Depth

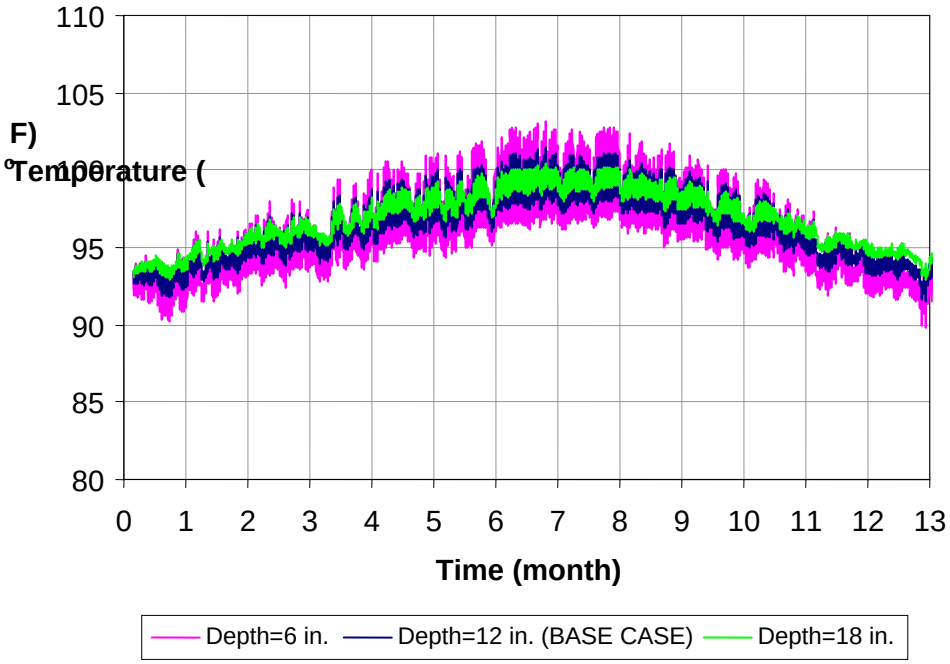

Figure 5. Sensitivity to Pipe Spacing

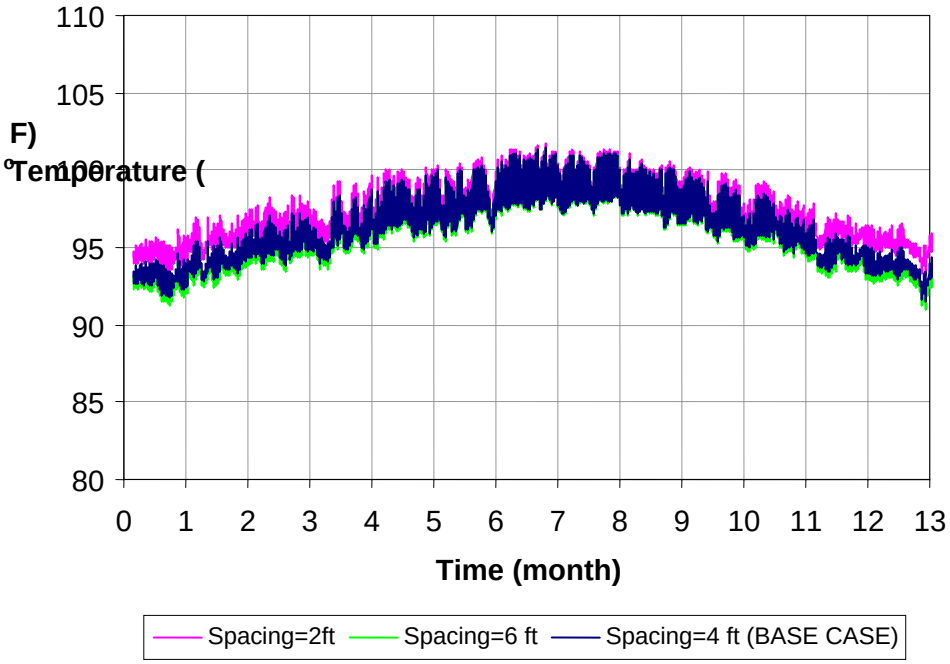

APPENDIX A

MODEL DOCUMENTATION

A Model for Simulating the Performance of a Pavement Heating System as a Supplemental Heat Rejecter With Closed-Loop Ground-Source Heat Pump Systems

Andrew D. Chiasson
Jeffrey D. Spitler
Simon J. Rees

School of Mechanical and Aerospace Engineering, Oklahoma State University, Stillwater, OK 74078

Marvin D. Smith
Division of Engineering Technology, Oklahoma State University, Stillwater, OK 74078

The thermal loads of commercial and institutional buildings are generally cooling-dominated. When such buildings use ground source heat pump systems (GSHP) they reject more heat to the ground-loop heat exchanger than they extract over the annual cycle. In these situations, supplemental heat rejecters can be used to reduce the required size of the ground-loop heat exchanger, thereby reducing the first cost of the system. This paper describes the development, validation, and use of a design and simulation tool for modeling the performance of a hydronic pavement heating system as a supplemental heat rejecter in ground-source heat pump systems. The model uses a finite difference method to solve the transient two-dimensional heat conduction equation and has been formulated for use in component based system simulation. Full-scale experiments were conducted concurrently with the development of the model, the results of which have been used for validation purposes. An example application simulation is presented to demonstrate the use of the model as well as the viability of the use of pavement heating systems as supplemental heat rejecters in GSHP systems. [S0199-6231(00)00404-4]

1 Introduction

Ground source heat pump (GSHP) systems have become increasingly popular for residential, commercial, and institutional heating and cooling applications because of their higher thermal efficiency compared to conventional systems using the outside air as a heat sink. In closed-loop GSHPs, heat rejection/extraction is accomplished by circulating a heat exchange fluid (usually water or an antifreeze mixture) through high-density polyethylene (HDPE) pipe buried in horizontal trenches or vertical boreholes. In large-scale commercial applications, vertical borehole systems are preferred over horizontal trench systems because less ground area is required.

The thermal loads of commercial and institutional buildings are often dominated by cooling requirements. Such buildings reject more heat than they extract over the annual cycle and often reject heat during large parts of winter days. In order to adequately dissipate the imbalanced annual loads, the required ground-loop heat exchanger lengths are significantly greater than the required length if the annual loads were balanced. Consequently, under these circumstances, ground-source heat pump systems may be eliminated from consideration during the feasibility study phase of the HVAC design process because of excessive first cost.

To effectively balance the ground loads and reduce the necessary size of the ground loop heat exchanger, supplemental components can be integrated into the ground-loop heat exchanger design. The supplemental heat exchanger can be taken advantage of in off-season periods and often in the early and late hours of the day (including summer days). GSHP systems that incorporate some type of supplemental heat rejecter are commonly referred to as hybrid GSHP systems. Hybrid GSHP systems may include a cooling tower, fluid cooler, or cooling pond. In applications where the excess heat that would otherwise build up in the ground is beneficial, domestic hot water heaters, car washes, or hydronic pavement heating systems can also be used. In buildings whose thermal loads are dominated by cooling requirements—where it may be necessary to reject heat on winter days—hydronic pavement heating systems have an additional benefit in that they may be used to provide a cost-effective means for pavement de-icing.

The objective of this work has been to develop a design and simulation tool for modeling the performance of a hydronic pavement heating system that can be usefully and cost-effectively integrated into a ground-source heat pump system as a supplemental heat rejecter. The model has been developed for use in component-based system simulation environments such as TRNSYS [1] and HVACSIM+ [2], where it can be coupled to other GSHP system component models. Experiments were conducted over several months using a full-scale heated pavement slab and embedded pipe loop. An attempt has been made to validate the model using the transient experimental data. As an example of the model's applicability, GSHP system simulation results are presented for a commercial building located in Tulsa, Oklahoma with a hypothetical closed-loop GSHP system with and without a pavement supplemental heat rejecter.

2 Heat Transfer in Pavement Slabs

Hydronically-heated pavement systems commonly use one of two types of pipe configurations: the ''serpentine'' configuration or the ''slinky'' configuration. The serpentine configuration (Fig. 1) is that commonly used in snow-melting systems. The pipes are embedded in the pavement material and are placed on even centers and connected with U-shaped tubing. In the slinky configuration (Fig. 2), a pipe is coiled in a circular fashion such that each loop overlaps the adjacent loop. The slinky is typically installed in fill material near the base of the pavement slab.

Contributed by the Solar Energy Division of The American Society of Mechanical Engineers for publication in the ASME JOURNAL OF SOLAR ENERGY ENGINEERING. Manuscript received by the ASME Solar Energy Division, Jan. 2000; final revision, Sep. 2000. Associate Technical Editor: V. C. Mei.

 Copyright © 2000 by ASME

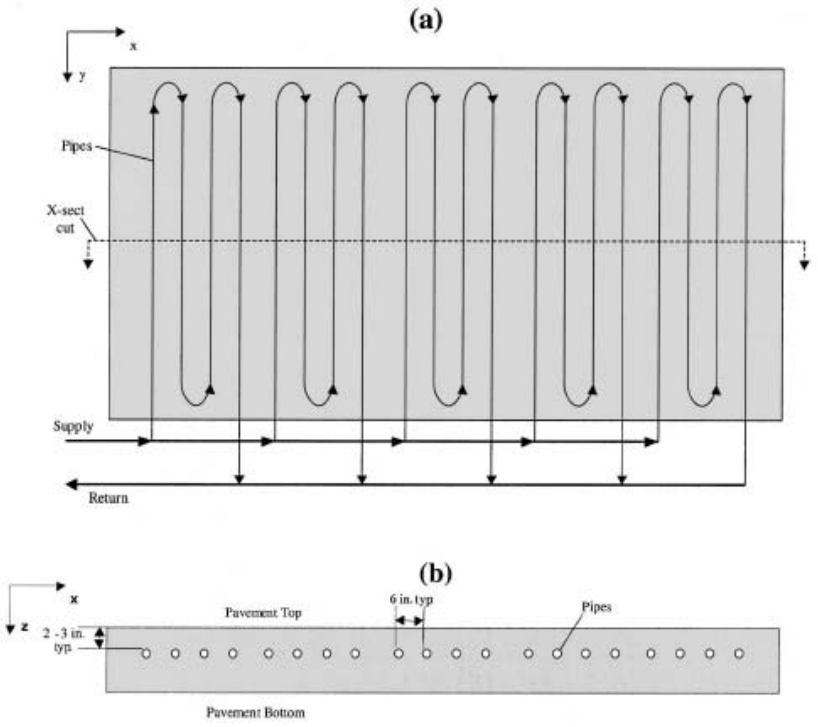

Fig. 1 Serpentine pipe configuration in a hydronically-heated pavement slab in (*a*) plan view and (*b*) cross-sectional view

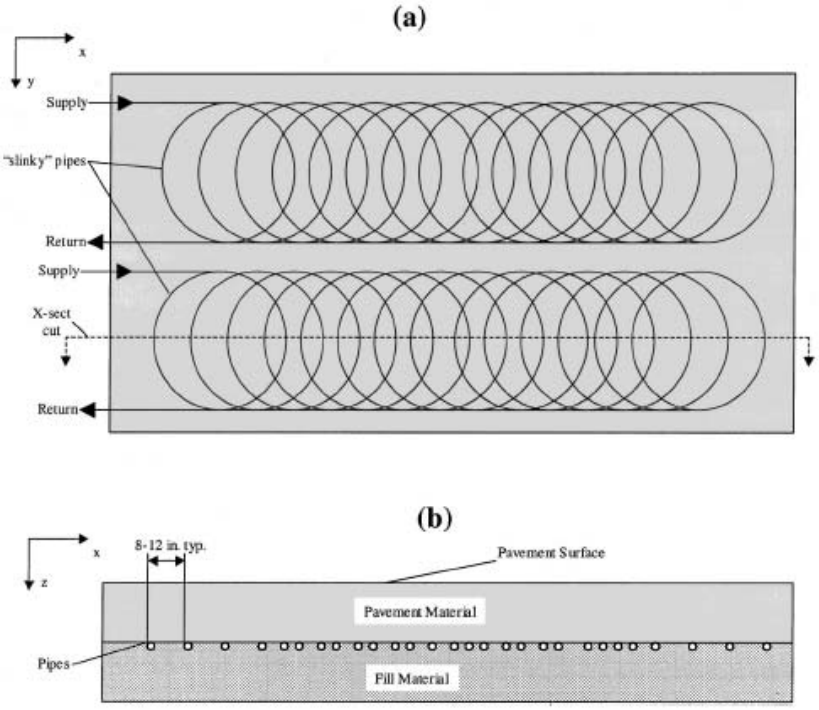

Fig. 2 Slinky pipe configuration in a hydronically-heated pavement slab in (*a*) plan view and (*b*) cross-sectional view along the slinky centerline

The principal heat transfer mechanisms in pavement slabs have been addressed by a number of authors in connection with snow melting applications [3–7]. Heat transfer within the slab itself is by conduction. Heat is transferred to the slab by convection from the flow of the heat transfer fluid through the pipes. Heat fluxes at the pavement surface are due to a number of environmental interactions and include convection, solar radiation, thermal (long-wave) radiation, sensible heat transfer from precipitation, and latent heat transfer from melting snow and evaporating water. On the bottom and sides of the slab, heat fluxes are due to conduction to the ground and may or may not be significant as compared to the top surface heat fluxes. If the slab bottom is exposed, as in the case of a bridge or parking deck, heat transfer from the bottom surface is by convection and long-wave radiation. Edge losses may be noticeable in slabs of sidewalk proportions but are not otherwise thought to be significant.

3 Experimental Methods

3.1 Test Slab Description and Data Collection. A hydronically-heated concrete slab has been constructed on a test site at the Oklahoma State University, Stillwater, OK and used for this study. The slab is rectangular with a plan area of 12.19 m (40 ft) by 1.22 m (4 ft) and a thickness of 152 mm (6 in.). The slab was underlain by 152 mm (6 in.) of sand fill material. The heat exchanger coil consisted of a single slinky coil installed at the concrete/sand fill interface.

The heat exchanger pipe is HDPE plastic and is 152.4 m (500 feet) long with a nominal diameter of 19.05 mm (0.75 in.). The pipe was coiled such that the resulting slinky heat exchanger is 12.19 m (40 ft) long with a diameter of 0.91 m (3 ft) and a 254 mm (10-in.) pitch (the separation distance between the apex of each successive loop).

An electric heating element in the hydronic system was used as the heat source and controlled to maintain a set water temperature of 23.9°C (75°F) entering the heat exchanger. The temperature of the concrete surface was measured by two thermistors embedded in the concrete at a depth of approximately 6.35 mm (0.25 in.) from the surface. One thermistor was placed near the center between two pipes of the slinky and the other was placed near the end above a pipe. Supply and return water temperatures were measured by thermistors embedded in the header pipe adjacent the slab. Flow rates were measured with an electronic flow meter and heat rejected to the fluid stream was measured with a watt transducer. All sensor information was recorded at time intervals of 6 min. over several weeks during November and December 1998.

3.2 Weather Instrumentation and Data Collection. Weather data for this study were obtained from the Oklahoma Mesonet (**meso**scale **net**work), an automatic weather station network with measurement stations throughout Oklahoma [8]. Data are recorded at time intervals ranging from 3 to 30 s. and averaged over 5-min. observation intervals. Weather data from the Stillwater monitoring station, located approximately 1 mile from the test site, were acquired for this study. Measurements of the following parameters were obtained: wind speed, wind direction, air temperature, relative humidity, and solar radiation.

4 Model Development

4.1 Governing Equations. Transient heat transfer in the pavement slab is represented in the model in two-dimensions. The cross-section is taken through the mid-section of the slab along the major direction of fluid flow in the pipe system and takes advantage of the vertical lines of symmetry through each pipe and between each pipe. This approach allows calculation of conditions representative of most of the slab but does not explicitly take into account edge losses. The transient two-dimensional heat conduction equation can be expressed as:

$$\frac{\partial^2 T}{\partial x^2} + \frac{\partial^2 T}{\partial z^2} = \frac{1}{\alpha}\frac{\partial T}{\partial t} \tag{1}$$

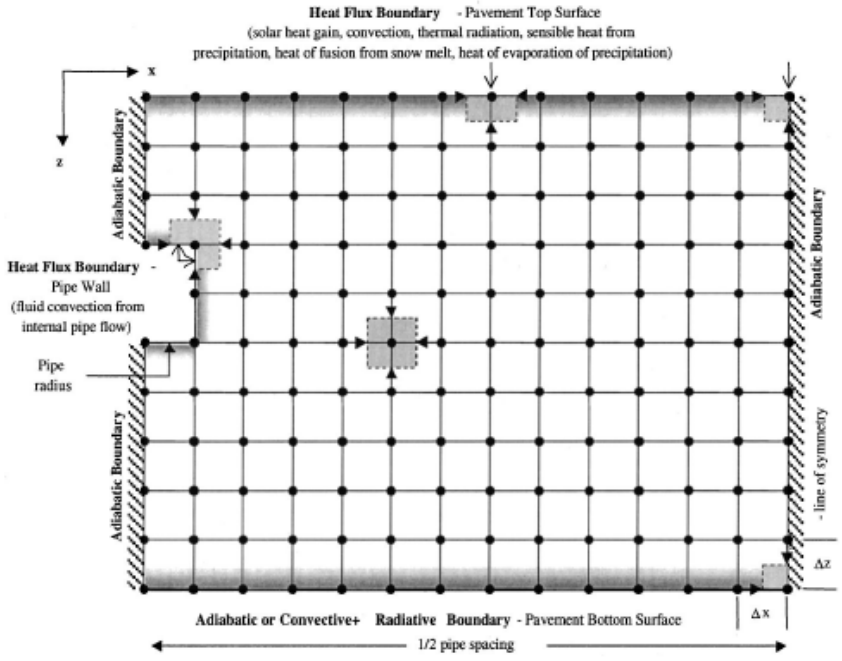

Fig. 3 Model domain showing the finite-difference grid and boundary conditions. Shaded squares show example control volumes for different types of grid node geometries

This equation has been discretized on an orthogonal Cartesian grid using an explicit finite difference method. The nodal equations are formulated in the *x-z* Cartesian coordinate plane using a node-centered, energy balance method.

4.2 The Finite Difference Grid. The finite difference grid used in the model is shown in Fig. 3. A uniform square nodal spacing equal to the pipe radius has been used. The grid domain has a width equivalent to one-half of the pipe spacing. In the vertical (z) direction, the domain extends from the top of the slab to the bottom of the slab (in the case of a suspended slab) or the base of the underlying fill material (in the case of a ground coupled slab). In the horizontal (x) direction, the domain corresponds to a distance from the centerline of a pipe to half the distance to the adjacent pipe.

4.3 Boundary Conditions. The boundaries of the model domain have flux-type (Neumann) boundary conditions as shown in Fig. 3. Lines of symmetry on the vertical boundaries are, by definition, zero-flux conditions. Heat flux at the pipe surface nodes represents convection from the heat transfer fluid. Heat flux at each top surface node ($q''_{(m,1)}$) is given by:

$$q''_{(m,1)} = q''_{solar} + q''_{long\text{-}wave} + q''_{convection} + q''_{rain,snow\text{-}sensible} + q''_{rain,snow\text{-}latent} \quad (2)$$

where q''_{solar} is the solar radiation heat flux, $q''_{long\text{-}wave}$ is the long-wave radiant heat flux, $q''_{convection}$ is the convective flux, $q''_{precipitation\text{-}sensible}$ is the sensible heat flux from falling rain and snow, and $q''_{precipitation\text{-}latent}$ is the latent heat flux from melting snow and evaporating/condensing water. The bottom surface is treated either as an adiabatic surface or, when exposed, with convection and long-wave radiation boundary conditions similar to the top surface. Each of the heat flux terms is further described below.

4.3.1 Solar Radiation Heat Flux. Solar radiation heat flux (q''_{solar}) is the net solar radiation absorbed by the pavement surface and is given by:

$$q''_{solar} = \alpha I \quad (3)$$

where I is the total (beam and diffuse) solar radiation incident on the pavement surface and α is the solar absorptivity of the pavement material. The absorptivity coefficient is corrected for solar incidence angle (υ) dependence using an empirical correlation given by Duffie and Beckman [9]. The model also accepts (if the weather data allows) solar radiation in the form of direct-normal/beam (I_b) and diffuse (I_d) components, in which case:

$$I = I_b \cos\theta + I_d \quad (4)$$

The angle of incidence is computed at each time step from correlations given by Spencer [10], Duffie and Beckman [9], and ASHRAE [11].

4.3.2 Long-wave Radiation Heat Flux. This heat transfer mechanism accounts for heat flux at the pavement top surface and bottom surface (if exposed) due to thermal or long-wave radiation. This model uses a linearized radiation coefficient (h_r) defined as:

$$h_r = 4\varepsilon\sigma\left(\frac{T_{(m,n)} + T_2}{2}\right)^3 \quad (5)$$

where ε is the emissivity coefficient of the pavement material, σ is the Stefan-Boltzmann constant, $T_{(m,n)}$ is the surface node temperature in absolute units, and T_2 represents either the sky temperature or in the case of the lower surface being exposed, the ground temperature. In the latter case the ground temperature is approximated by the air dry bulb temperature. T_{sky} is computed from the relationship given by Bliss [12], which correlates sky temperature with dew point (T_{dp}) and dry bulb (T_{db}) temperatures:

$$T_{sky} = T_{db}\left(0.8 + \frac{T_{dp}}{250}\right)^{1/4} \quad (6)$$

The long-wave radiation heat flux at each node ($q''_{long\text{-}wave}$) is then computed by:

$$q''_{long\text{-}wave} = h_r(T_2 - T_{(m,n)}) \quad (7)$$

4.3.3. Convection Heat Flux at the Pavement Surfaces. Convection at the upper (and perhaps lower) surfaces is considered either free or forced in nature depending on the current wind conditions. The convection heat flux at each pavement surface node ($q''_{convection}$) is computed by:

$$q''_{convection} = h_c(T_{db} - T_{(m,n)}) \quad (8)$$

where h_c is the convection coefficient. We follow the practice recommended by Duffie and Beckman [10] and McAdams [13] in determining the effective convection coefficient by taking the larger of the coefficients calculated for free and forced convection conditions at each time-step.

We make use of the convection correlations for flat plates given in Incropera and DeWitt [14]. For free convection conditions the correlation is $Nu = 0.54\ Ra^{0.25}$ where $10^4 < Ra < 10^7$, and $Nu = 0.15\ Ra^{0.333}$ where $10^7 < Ra < 10^{11}$. For forced convection conditions the correlations are $Nu = 0.664\ Re^{0.5}\ Pr^{0.333}$ where $Re < 2000$ and $Nu = 0.037\ Re^{0.8}\ Pr^{0.333}$. The Reynolds Number is calculated at each time step using the windspeed data and taking the characteristic length as the ratio of the slab length (parallel to the wind direction) to the perimeter. The value of Ra is calculated using the difference between the current value of slab surface node temperature and dry bulb temperatures. Subsequently h_c in equation 8 is taken as the largest of the calculated coefficients.

4.3.4 Heat Flux Due to Precipitation. This heat transfer mechanism includes both sensible and latent effects. This model uses a simple mass/energy balance on water at the pavement surface to account for heat and mass transfer. The sensible heat flux due to falling rain or snow at each pavement surface node ($q''_{precipitation}$) is given by:

$$q''_{precipitation} = \dot{m}''_{precipitation} c_p (T_{db} - T_{(m,1)}) \quad (9)$$

where $\dot{m}''_{precipitation}$ is the rainfall or snowfall rate in water equivalent mass per unit time per unit area and c_p is the specific heat capacity of water at the air temperature.

Latent heat transfer is considered only if the air temperature or the slab surface temperature is above 33°F (0.55°C). Accumulation of rain is not considered; rainfall is assumed to drain instantaneously from the pavement surface, forming a thin film from which evaporation occurs.

This model uses the *j*-factor analogy to compute the mass flux of evaporating water at each pavement surface node ($\dot{m}''_w$):

$$\dot{m}''_w = h_d(w_{air} - w_{(m,1)}) \quad (10)$$

where h_d is the mass transfer coefficient, w_{air} is the humidity ratio of the ambient air, and $w_{(m,1)}$ represents the humidity ratio of saturated air at the surface node. The mass transfer coefficient (h_d) is defined using the Chilton-Colburn analogy, $h_d = h_c/(c_p\ Le^{2/3})$ where h_c is the convection coefficient defined above, c_p is the specific heat capacity of the air evaluated at the pavement node–air film temperature, and Le is the Lewis number. The heat flux due to evaporation ($q''_{evaporation}$) is then given by:

$$q''_{evaporation} = h_{fg} \dot{m}''_{w} \quad (11)$$

where h_{fg} is the latent heat of vaporization and is computed from the relationship given by Irvine and Liley [15].

The heat flux due to melting snow and ice is determined using a mass balance on freezing precipitation that has accumulated at the pavement surface. The accumulation of ice at the beginning of each time step is determined from the sum of the rainfall rate and the snowfall rate if the air temperature or the slab surface temperature is below 0.55°C (33°F). Although snow is a porous medium, it is treated in the model as an equivalent ice layer. Sublimation of ice is not considered. The mass flux of water due to melting ice ($\dot{m}''_{icemelt}$) at the pavement surface is then given by:

$$\dot{m}''_{icemelt} = (q''_{solar} + q''_{thermal} + q''_{convection} + q''_{rain,snow\text{-}sensible} + q''_{evaporation} + q''_{conduction,ice})/h_{if} \quad (12)$$

where $q''_{conduction,ice}$ is the conduction heat flux from the pavement surface into the ice layer and h_{if} is the latent heat of fusion of water. The other heat flux terms have been defined previously. If the ice thickness is greater than zero, the heat flux into each pavement surface node ($q''_{(m,1)}$) is given by:

$$q''_{(m,1)} = -\dot{m}''_{icemelt} h_{if} \quad (13)$$

4.3.5 Heat Transfer with the Heat Exchange Fluid. Heat transfer with the heat exchange fluid is represented by heat flux at the pipe surface nodes. The thermal properties of the fluid are computed at each time step from correlations given in the *Handbook of Chemistry and Physics* [16] for water and from correlations given by Wadivkar [17] for an antifreeze solution. The thermal properties are computed at the average fluid temperature (T_{fluid}), which is the average of the inlet and outlet temperatures at each given time step. Since the outlet temperature at any current time step is not known, the calculation of T_{fluid} is iterative.

The heat flux due to the heat exchange fluid (q''_{fluid}) is computed per flow circuit by:

$$q''_{fluid} = U_{pipe}(T_{fluid} - T_{(m,n)}) \quad (14)$$

where U_{pipe} is the overall heat transfer coefficient (i.e., including inside and outside convective conductances) for the pipe which is computed at each time step.

The outlet fluid temperature (T_{out}) is computed from an overall energy balance on the pipe flow circuit:

$$T_{out} = T_{fluid} - \frac{q''_{fluid} A_{pipe}}{2\dot{m} c_p} \quad (15)$$

where A_{pipe} is the inside surface area of the pipe per flow circuit and $\dot{m}$ is the mass flow rate of the heat exchange fluid per flow circuit.

5 Results and Discussion

5.1 Model Comparison to Experimental Results. Heat rejection to the test slab was simulated over a 36-day period from November 12 to December 18, 1998 (during which there was some rain but no snow). Input data to the model consisted of actual weather data in addition to measured slab supply water temperatures and flow rates. In order to deal with the fact that the experiment used a slinky pipe configuration where the pipe spacing is not uniform [Fig. 2(*b*)] a heuristic approach was used to determine an effective pipe spacing along the centerline of the coil. For a slinky with a 254 mm (10-inch) pitch, an effective pipe spacing of 210 mm (8.4 in.) was determined by taking the arithmetic average of the pipe spacing at the points of overlap.

The model performance was evaluated by comparing (i) the simulated to the observed return temperature of the heat exchange fluid and (ii) the simulated cumulative heat rejected to the measured water heating element and pump power input. These comparisons are shown in Fig. 4. During the 36-day test period, the weather changed from being initially dry, clear and warm (13 November to 28 November), then rainy and overcast (29 November to 6 December), to a final period of about 14 days when the dry-bulb temperature was significantly lower (7 December to 18 December). There was only 0.25 mm (0.01 in) of rain during the initial 16 days. Between 30 November and 6 December there was considerable rain—totaling 61 mm (2.4 in). A notable drop in fluid return temperature occurred on the 6 December [Fig. 4(*a*)] corresponding to the significant drop in dry-bulb temperature.

The predicted return temperatures follow the measured diurnal fluctuations as well as the previously noted drop in return temperature on 6 December due to the arrival of a cold weather front [Fig. 4(*a*)]. During the whole test period the model return water temperature deviated from the measured temperature by an average of 0.45°C (0.82°F). The average observed and modeled fluid return temperatures over the test period were 22.8°C (73.1°F) and 23.0°C (73.4°F), respectively.

The record of the cumulative power dissipated by the heat exchanger system shows a reasonably constant rate of output except for a slightly reduced rate of output during the period 29 November to 6 December [Fig. 4(*b*)]. This reduction in output is over predicted by the model, as shown by a more noticeable reduction in slope of the cumulative power graph during this period. It can be seen from Fig. 4(*a*) that the diurnal variations in fluid temperature are also reduced during this period. This can be expected due to reduced nighttime radiation to the sky with increased cloud cover. The measured output is likely to be higher than that predicted by the model due to the high rainfall recorded during this period. The clay soil at the experimental site, as well as the layer of sand below the slab, was relatively dry at the start of the test and became very saturated during the period of high rainfall. Although sensible and evaporative losses due to precipitation are accounted for in the model, there is no way to account for conditions where the surrounding ground may become saturated and losses to the ground are enhanced by increased conduction and convection. Nevertheless, the accuracy of the overall heat rejection prediction is acceptable for the models intended purpose. At the end of the 36-day test period, the percent difference between the cumulative simulated heat rejected and the cumulative measured heat rejected was −4.71 percent.

5.2 Model Uncertainty Analysis. A model sensitivity analysis was conducted to quantify the uncertainty in the final model results caused by uncertainties in the estimates of input and parameter values used in the models. The model uncertainty was quantified using influence coefficients [18]. An influence coefficient is the partial derivative of a *simulation result* with respect to a *parameter*. For this study, the *simulation result* is the cumulative heat rejected and the *parameter* is any variable with some uncertainty.

The parameters investigated in this uncertainty analysis can be divided into model parameters and model inputs. The model parameters considered in this analysis were: (a) pipe thermal conductivity, (b) concrete thermal conductivity, (c) underlying soil thermal conductivity, (d) absorptivity of the concrete surface and (e) emissivity of the concrete surface. The model inputs considered in the analysis were: (a) wind speed, (b) air temperature, (c) relative humidity, (d) supply fluid temperature, and (e) supply fluid flow rate.

The supply fluid temperature was found to have the greatest effect on the model uncertainty, on the order of 8 percent. The absorptivity of the concrete surface possesses the next highest uncertainty, on the order of 5 percent. The uncertainties in the air temperature, soil thermal conductivity, and emissivity of the con-

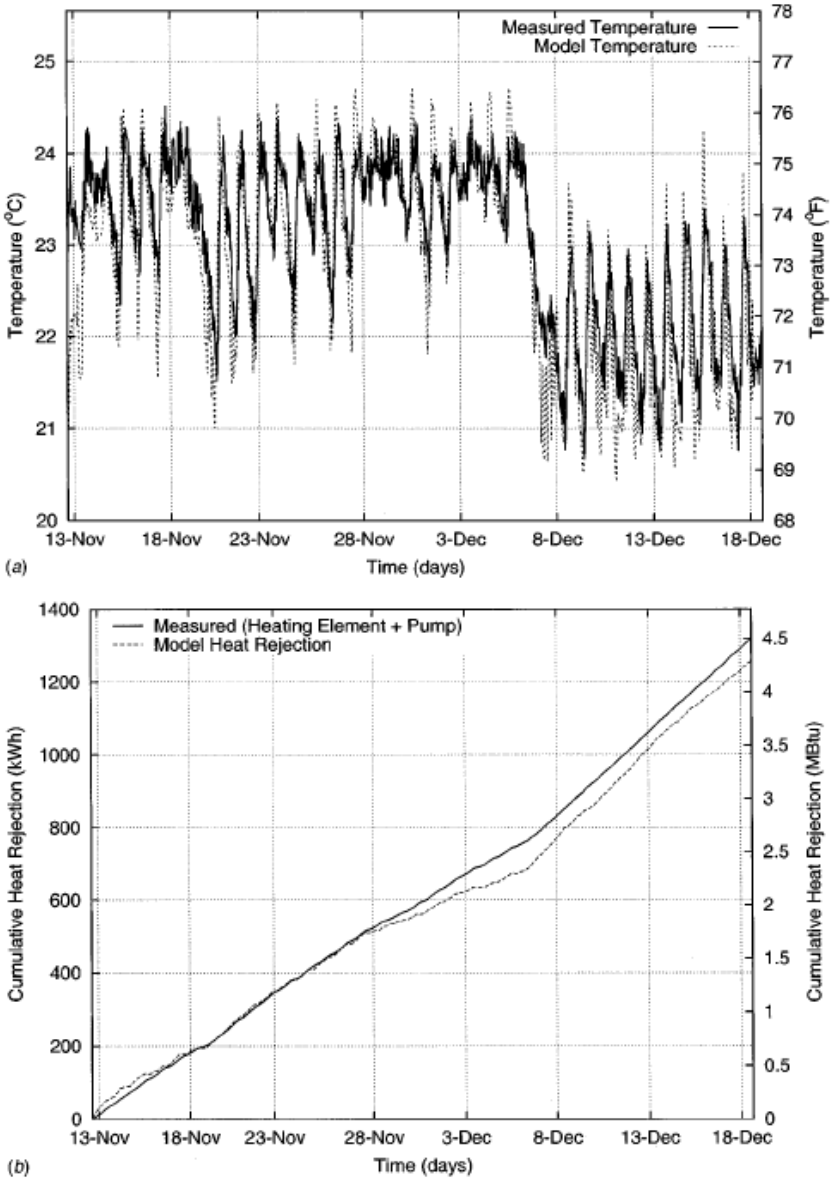

Fig. 4 Compairson of observed and simulated (*a*) heat exchange fluid return temperature and (*b*) heat rejected to the parking lot test section

crete surface are estimated to produce uncertainties in the cumulative heat rejection on the order of 2.5 percent. Uncertainties in the pipe thermal conductivity and the concrete thermal conductivity are likewise estimated to produce uncertainties of 1.7 percent and 0.8 percent, respectively, in the cumulative heat rejection. The wind speed and relative humidity have relatively low sensitivities on the order of 0.5 percent. The fluid flow rate has an insignificant effect on the model uncertainty, contributing only 0.03 percent to the total. These uncertainties are assumed to be independent of each other, yielding a total uncertainty in the predicted cumulative heat rejection of ±10.47 percent. Further details of the uncertainty calculations can be found in Chiasson [19].

6 Model Application

To illustrate the applicability of the model as well as the viability of using pavement heating systems as supplemental heat rejecters in GSHP systems, a model of a hypothetical GSHP system was constructed in the TRNSYS modeling environment [1]. A simplified system schematic is shown in Fig. 5. For this example, a pavement heating system similar to the test section described above was used. Each of the component models is described briefly below.

The building is not modeled explicitly in this application. The hourly building thermal loads are pre-computed using a building

energy analysis program and used as boundary conditions for the simulation. The building is an actual four-story, 4181 m^2 (45,000 ft^2) office building located in Tulsa, Oklahoma and is highly cooling dominated, with a peak cooling load of 352 kW.

A simple water-to-air heat pump model was developed for this type of GSHP system simulation. The model uses quadratic curve-fit equations to manufacturer's catalog data to compute the heat of rejection, heat of absorption, and power consumption. Inputs to the model include the hourly building loads, entering fluid temperature, and fluid mass flow rate. Outputs computed by the model include exiting fluid temperature and power consumption.

The ground-loop heat exchanger model used in this application is that described by Yavuzturk and Spitler [20]. This model extends the work of Eskilson [21] to hourly or less time intervals using short time-step response factors derived from a detailed borehole model [22]. In this application, the modeled borehole field consisted of one hundred 76.2 m (250 ft) deep boreholes arranged in a 10 by 10 square pattern. A total system flow rate of 17.0 L/s (270 gpm) was assumed. Representative thermal properties of sedimentary rock were chosen.

Ancillary components such as pumps, t-pieces, flow diverters, and the differential controller are found in the TRNSYS library [1]. The strategy used to control flow through the pavement was based on the temperature difference between the pavement surface and the exiting fluid temperature from the heat pumps. When this temperature difference exceeds a somewhat arbitrarily chosen

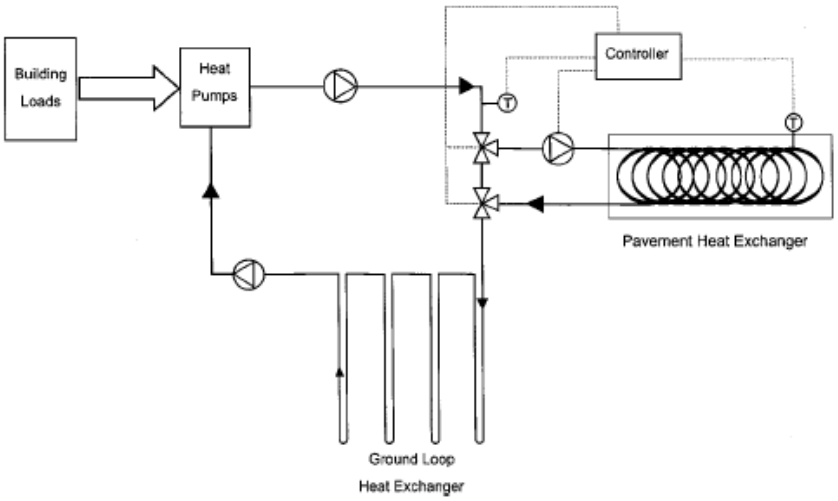

Fig. 5 System schematic for the example model of a GSHP system with a pavement heating system supplemental heat rejecter

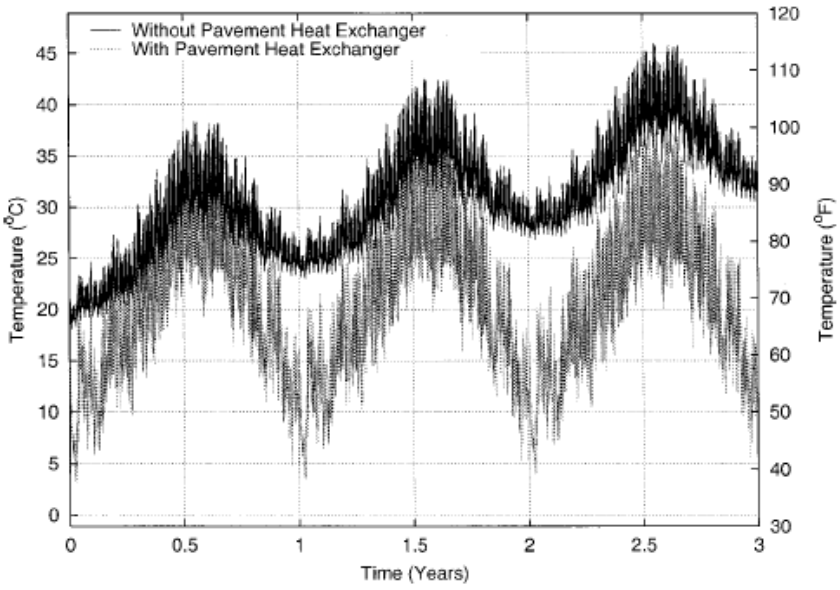

Fig. 6 Entering heat pump water temperatures for the example GSHP system simulation with no pavement heating and with a 2230 m^2 (24,000 ft^2) parking lot with pavement heating

temperature of 5°C (9°F), the circulating pump to the pavement is energized and flow is diverted to the pavement system. The properties of each heat exchanger coil in the example model are the same as those described in the test section experiments. Hourly input weather data for the model were taken from a typical meteorological year (TMY) record for Tulsa, Oklahoma.

Two cases were simulated over a duration of 3 years using a model time step of one hour. In the first case, the GSHP system used only the borehole field as a heat sink. In the second case, both the borehole field and pavement slab were used. For the second case, it was assumed that a maximum heat pump entering fluid temperature of 37.8°C (100°F) was desirable and that the 10 by 10 borehole field could not be feasibly deeper than 76.2 m (250 feet). Using the TRNSYS model as a design tool, a 2230 m^2 (24,000 ft^2) pavement area with 200 slinky heat exchanger coils was found to produce acceptable heat pump entering fluid temperatures. Hourly heat pump entering water temperatures are shown in Fig. 6 for both cases.

A review of the data presented in Fig. 6 shows the advantages of using a pavement heating system as a supplemental heat rejecter. With the pavement heat exchanger in operation, the peak annual entering water temperature is shown to be similar each year. With only the borehole field in operation the peak annual entering water temperature rises each year up to about 46°C (115°F) in the third year. Accordingly, using a supplemental heat exchanger such as this can result in a significantly reduced borehole field size. Based on the results of a ground-loop heat exchanger design program [23], the boreholes of a 10 by 10 square pattern would need to be approximately 121.9 m (400 feet) deep to accommodate the cooling dominated loads of this building for 20 years of operation. Therefore, by adding the pavement supplemental heat rejecter in this example, the depth of the borehole field can be decreased by approximately 35 percent.

It should also be noted that the task of sizing a supplemental heat rejecter is something of an optimization problem with several degrees of freedom. Use of models such as this in simulation offers a reasonable way of assessing the overall system dynamic behavior.

7 Conclusions and Recommendations

A design and simulation tool for modeling the performance of a pavement heat exchanger has been developed. Such heat exchangers may be useful as supplemental heat rejecters in hybrid ground-source heat pump systems. The model has been developed for use in component based system simulation environments and can be coupled to other GSHP system component models for short time-step system analyses. Data from a full-scale experimental pavement heat exchanger has been used to test the validity of the model with some success.

The model accounts for the principal environmental heat transfer mechanisms and coupling to the hydronic pipe loop. The model uses a finite-difference method to solve the transient two-dimensional heat conduction equation. Outputs provided by the model include the pavement surface temperature, the exiting fluid temperature, and the amount of heat rejected to the pavement slab. The performance of the model has been evaluated against data collected from an experimental pavement heat exchanger. The model was found able to predict the heat exchanger return fluid temperatures with acceptable accuracy.

An example application has been presented to demonstrate the use of the model as well as the viability of the use of pavement areas as supplemental heat rejecters in GSHP systems. In addition the model is sufficiently generalized that it can be used to model slabs used in heated bridge decks or as simple solar collectors. Further research is suggested in the following areas:

- Optimization of the design procedure and control strategy when used in a GSHP system.
- Additional validation of the model under a wider range of conditions such as snow precipitation.
- Study of the impact of the pipe configuration on system performance.

Acknowledgments

This work was supported by the U.S. Department of Energy through contract awards DE-FG48-97R810627 and DE-FG48-94R689416. Support by the Department of Energy does not constitute endorsement of the views expressed in this article.

Nomenclature

A = area, m^2 (ft^2)
c_p = specific heat capacity, J/kg-°C (BTU/lb.°F)
h = heat or mass transfer coefficient, W/m^2-°C (BTU/h.ft^2.°F)
I = solar radiation, W/m^2 (BTU/h.ft^2)
k = thermal conductivity, W/m-°C (BTU/h.ft.°F)
$\dot{m}$ = mass flow rate, kg/s (lb/h)
q'' = heat flux, W/m^2 (BTU/h.ft^2)
q = heat transfer rate, W (BTU/h)
t = time, s (h)
T = temperature, °C (°F)
U = overall heat transfer coefficient, W/m^2-°C (BTU/h.ft^2.°F)

Greek Symbols

α = thermal diffusivity, m^2/s (ft^2/h) and solar absorptivity (-)
ε = emissivity coefficient (-)
σ = Stephan-Boltzmann constant

Subscripts

c = convection
$fluid$ = heat transfer fluid average property
in = inlet
m,n = coordinate locations
out = outlet
r = thermal radiation
(m,n) = coordinate locations

References

[1] Solar Energy Laboratory (SEL), University of Wisconsin-Madison, 1997, "TRNSYS, A Transient Systems Simulation Program, User's Manual," Version 14.2.
[2] Clark, D. R., and May, W. B., 1985, "HVACSIM+ Building System and Equipment Simulation Program–Users Guide," National Bureau of Standards.
[3] Adlam, T. N., 1950, *Snow Melting*, The Industrial Press, New York, NY.
[4] Chapman, W. P., 1952, "Design of Snow Melting Systems," Heat. Vent., April, **49**, pp. 96–102.
[5] Kilkis, I. B., 1994, "Design of Embedded Snow Melting Systems: Part 1, Heat Requirements—An Overall Assessment and Recommendations," ASHRAE Trans., **100**, No. 1, pp. 423–433.
[6] ASHRAE, 1999, *ASHRAE Handbook*, HVAC Applications: Chapter 49, "Snow Melting," American Society of Heating, Refrigeration and Air Conditioning Engineers, Inc., Atlanta, GA.
[7] Ramsey, J. W., Hewett, M. J., Kuehn, T. H., and Petersen, S. D., 1999, "Updated Design Guidelines for Snow Melting Systems," ASHRAE Trans., **105**, No. 1, 1055–1065.
[8] Elliott, R. L., Brock, F. V., Stone, M. L., and Sharp, S. L., 1994, "Configuration Decisions for an Automated Weather Station Network," Appl. Eng. Agricul., **10**, No. 1, pp. 45–51.
[9] Spencer, J. W., 1971, "Fourier Series Representation of the Position of the Sun," J. Australian New Zealand Assoc. Adv. Sci., 2, No. 5, p. 172.
[10] Duffie, J. A., and Beckman, W. A., 1991, *Solar Engineering of Thermal Processes*, 2nd Edition, John Wiley and Sons, New York.
[11] ASHRAE, 1997, *ASHRAE Handbook*, Fundamentals: Chapter 29, "Fenestration," American Society of Heating, Refrigeration and Air-Conditioning Engineers, Inc., Atlanta, GA.
[12] Bliss, R. W., 1961, "Atmospheric Radiation Near the Surface of the Ground," Solar Energy, **5**, No. 3, pp. 103–120.
[13] W. H. McAdams, 1954, *Heat Transmission*, 3rd Edition, McGraw-Hill Book Company, New York.

[14] Incropera, F. P., and DeWitt, D. P., 1996, *Introduction to Heat Transfer*, 3rd Edition, John Wiley & Sons, New York.
[15] Irvine, T. F., Jr., and Liley, P. E., 1984, *Steam and Gas Tables with Computer Equations*, Academic Press, Inc., New York.
[16] Chemical Rubber Company (CRC), 1980, *Handbook of Chemistry and Physics*, 61st Edition, CRC Press, Cleveland, OH.
[17] Wadivkar, O., 1997, An Experimental and Numerical Study of the Thermal Properties of a Bridge Deck De-Icing System, Masters Thesis, Oklahoma State University, Stillwater, OK.
[18] Spitler, J. D., Fisher, D. E., and Zietlow, D. C., 1989, "A Primer on the Use of Influence Coefficients in Building Simulation," *Proc. of Building Simulation '89*, Vancouver, BC.
[19] Chiasson, A. D., 1999, Advances in Modeling of Ground-Source Heat Pump Systems, Masters Thesis, Oklahoma State University, Stillwater, OK.
[20] Yavuzturk, C., and Spitler, J. D., 1999, "A Short Time Step Response Factor Model for Vertical Ground Loop Heat Exchangers," ASHRAE Trans., **105**, No. 2, pp. 475–485.
[21] Eskilson, P., 1987, Thermal Analysis of Heat Extraction Boreholes, Doctoral Thesis, University of Lund, Department of Mathematical Physics, Lund, Sweden.
[22] Yavuzturk, C., Spitler, J. D., and Rees, S. J., 1999, "A Transient Two-Dimensional Finite Volume Model for the Simulation of Vertical U-Tube Ground Heat Exchangers," ASHRAE Trans., **105**, No. 2, pp. 465–474.
[23] Spitler, J. D., Marshall, C., Delahoussaye, R., and Manicham, M., 1996, Users Guide of GLHEPRO, Stillwater, OK, School of Mechanical and Aerospace Engineering, Oklahoma State University.